Asian Journal of Chemistry; Vol. 36, No. 11 (2024), 2647-2653

ASIAN JOURNAL OF CHEMISTRY

https://doi.org/10.14233/ajchem.2024.32635

Synthesis and Evaluation of Novel Ternary $MgFe_2O_4/CuO/TiO_2$ Nanocomposite for Visible Light Photodegradation of Malachite Green Dye

K. Jyothi Priya*, Ch. Ramya Kumari, M. Suneetha, G. Supriya, R. Goldina, M. Padma and S. Paul Douglas*

Department of Engineering Chemistry, AU College of Engineering, Andhra University, Visakhapatnam-530003, India

*Corresponding authors: E-mail: priya.konathala94@gmail.com; pauldouglas12@gmail.com

Received: 2 September 2024; *Accepted*: 22 October 2024; *Published online*: 30 October 2024; AJC-21803

Novel ternary $MgFe_2O_4/CuO/TiO_2$ nanocomposite was synthesized using the sol-gel method at low temperatures. The XRD, FTIR, SEM-EDX, TEM, UV-visible DRS and VSM techniques were used to characterize the structure, shape, optical, morphology and magnetic properties. The XRD examination revealed typical peaks in nanocomposites, including the anatase phase of TiO_2 with an average diameter of 9 nm, consistent with the TEM data. The SEM morphology examinations revealed spherical particles, while EDAX analysis indicated the corresponding components (Fe, Ti, O, Mg and Cu) in the prepared nanocomposites. The UV-DRS measurements revealed that the synthesized nanocomposite has a band-gap energy of 2.30 eV. The vibrating sample magnetometer (VSM) was used to trace the M-H loop of $MgFe_2O_4$, yielding magnetic parameters such as saturation magnetization (Ms). The catalytic activity of the as-prepared sample was examined by the degradation of malachite green dye under visible light and UV irradiations. The photocatalytic studies demonstrated that $MgFe_2O_4/CuO/TiO_2$ nanocomposite showed 100% degradation efficiency towards malachite green dye. Under visible light and UV irradiations, the synthesized $MgFe_2O_4/CuO/TiO_2$ sample with a molar ratio of 0.8:0.1:0.1 demonstrated good catalytic efficiency. The antibacterial activity investigations were done against Gram-negative *Escherichia coli*, *Klebsiella pneumonia*, Gram-positive *Staphylococcus aureus* and *Bacillus subtilis* bacteria utilizing nanocomposites.

Keywords: $MgFe_2O_4/CuO/TiO_2$ nanomagnetic composites, Visible-light photodegradation, Malachite green, Antibacterial studies.

INTRODUCTION

One of the primary environmental contamination challenges has been industrial wastewater, particularly from the textile and dye industries, which contains toxic effluents [1]. During the dying process, considerable quantities of synthetic dyes are lost to sewage (15% of total global dye output), eventually harming the environment [2]. Removing toxic dyes from rivers and wastewater treatment is of major significance from an environmental standpoint the depletion of water supplies caused by various dyes can damage natural ecosystems. TiO_2 is a well-known and effective photocatalyst for the removal of organic contaminants. Titania, a photocatalyst with good heterogeneous photocatalytic characteristics, high stability and low cost, has caught the curiosity of researchers [3,4]. But due to its expansive band gap energy (3.2 eV), TiO_2 is limited in practical applications for photocatalytic activities with catalysts under UV irradiation [5,6]. Studies have been focused on the innovative techniques to enhance the photocatalytic performance of TiO_2. To enable TiO_2 to absorb radiation in the visible part of the electromagnetic spectrum for various applications, researchers have been concentrating on doping lower band gap metal oxides to the material [5-7]. CuO is a p-type semiconductor with a 2.1-2.71 eV narrow band gap [8] and its nanoparticles react appropriately to mechanical, photolytic and optical applications [8,9].

Ferrite nanoparticles, MFe_2O_4, where M is any divalent metal ions such as Mg, Mn, Ni, Co, Fe, Cu, *etc*. find wide applications in several fields [10]. Ferrites typically have a maximum band gap energy of about 2 eV, which enables the materials to absorb visible light efficiently [11] and are commonly utilized as visible light photocatalysts to break down pollutants in water and wastewater [12]. Among numerous iron oxides, $MgFe_2O_4$, a member of the spinel family, offers a wide range of applications in electronic devices, heterogeneous catalysis, sensor technologies, *etc.* [12,13]. Because ferrites have magnetic

characteristics and may be separated from other substances in the catalytic process with a bar magnet, the inclusion of magnesium ferrite ($MgFe_2O_4$) overcomes the drawback of TiO_2, which is difficult to separate from the solution.

In present work, novel ternary $MgFe_2O_4/CuO/TiO_2$ nanocomposites were synthesized and analyzed for photocatalytic activity by measuring the degradation of malachite green dye under visible and UV light irradiation.

EXPERIMENTAL

Chemicals for synthesizing ternary $MgFe_2O_4/CuO/TiO_2$ nanocomposite and other solvents were obtained with AR grade quality from SD-Fine (99% purity). All the purchased materials were of analytical grade and used without further processing. All the reactions were carried out using deionized water.

Synthesis of $MgFe_2O_4$: The sol-gel technique was used for synthesizing $MgFe_2O_4$ magnetic particles. Added 20 mL of distilled water to each of 10.24 g of magnesium nitrate, 23.92 g of ferric citrate and 25.2 g of citric acid to dissolve and make standard solutions. Then, mixed magnesium nitrate and ferric citrate solutions followed by citric acid solution. NH_4OH solution was added to adjust the pH of the solution and poured in 20 mL of ethylene glycol. After stirring for 1 h, the solution was heated at 80 ºC until the contents become dry powder. It was then calcined at 500 ºC for 1 h, annealed at 500 ºC for 1 h and ground to a fine powder.

Synthesis of CuO: Copper nitrate (30 g) was dissolved in 20 mL of distilled water followed by 20 mL of ethylene glycol. The solution was stirred for 1 h and left for 1 day in order to obtain gel. The ingredients were then dried at 200 ºC till it become powder, which was calcined for 1 h at 300 ºC, annealed for 1 h at 500 ºC and ground to a fine powder.

Synthesis of TiO_2: In this synthesis, 6.9 mL of $TiCl_4$ (11.94 g) was gradually dispersed in 350 mL of distilled water under magnetic stirring for 30 to 60 min to allow complete hydrolysis, which results in the formation of a white curdy precipitate, orthotitanic acid. The resulting mixture was heated at 80 ºC to 100 ºC on an electrical hot plate and to obtain the powder. Finally, the powder was ground in a mortar and pestle and calcined for 2 h at 400 ºC [14].

$$TiCl_4 + H_2O \longrightarrow \underset{\text{(orthotitanic acid)}}{[Ti(OH)_4]} + H_2O$$

$$[Ti(OH)_4] \longrightarrow TiO_2 + 2H_2O$$

Synthesis of ternary $MgFe_2O_4/CuO/TiO_2$ nanocomposite: Ternary $MgFe_2O_4/CuO/TiO_2$ nanocomposite was synthesized by thoroughly mixing of above synthesized $MgFe_2O_4$, CuO and TiO_2 nanoparticles in a 0.8:0.1:0.1 ratio using a mortar and pestle.

Characterization: An X-ray diffractometer (Bruker DX-5) with $\lambda = 1.54$ Å at room temperature over a wide range of $10^\circ \le 2\theta \le 80^\circ$ at a scanning speed of 2 min^{-1} was used to analyze the phase of $MgFe_2O_4/CuO/TiO_2$ nanocomposite. The morphology of the ternary nanocomposite was studied with a field emission scanning electron microscopy (FESEM) instrument (Zeiss Gemini 300, Carl Zeiss, Germany). Fourier transform infrared (FTIR) spectroscopy (IR Prestige-21 instrument) was used to analyze the different functional groups of nanocomposite in the wavenumber range of 400-4000 cm^{-1}. Band gaps were determined using the Shimadzu 2600R with a 200-800 nm range and $BaSO_4$ as a reference.

RESULTS AND DISCUSSION

XRD spectral studies: The crystalline phase and purity were investigated using XRD analysis. The XRD pattern of $MgFe_2O_4/CuO/TiO_2$ is shown in Fig. 1. All of the observed prominent diffraction peaks are highly defined and may be assigned to the anatase phase TiO_2 at 2θ 26.6º, 36.4º, 48.7º, 54.2º, 61.5º (JCPDS card no: 21-1272), CuO at 2θ 32.4º, 38.7º, 68.8º, 73.4º (JCPDS card no: 48-1548) and $MgFe_2O_4$ at 2θ 30.16º, 35.5º, 43.1º, 56.9º, 62.7º (JCPDS card no: 73-2410). The diffraction peaks closely resemble the standard peaks of materials [15,16].

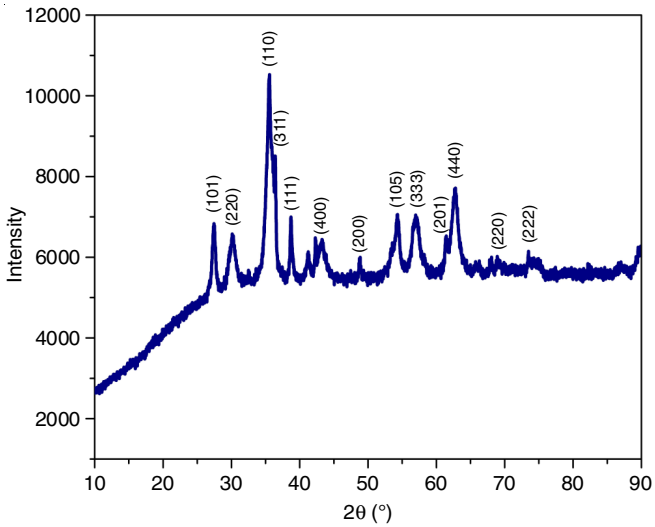

Fig. 1. XRD pattern of $MgFe_2O_4/CuO/TiO_2$

The average crystallite size of the sample was calculated by using The Debye-Scherrer's formula:

$$D = \frac{0.9\lambda}{\beta\cos\theta}$$

D represents the average size of crystals; 0.9 represents the grain's shape factor; λ corresponds to the X-ray wavelength; β indicates the full width at half maximum (FWHM) of the diffraction peak and θ represents the incident angle of X-ray. The average calculated crystal size of ternary $MgFe_2O_4/CuO/TiO_2$ nanocomposite was found to be 9 nm.

UV-Vis-DRS analysis: The ultraviolet-visible-diffuse reflectance spectroscopy (UV-Vis-DRS) absorption spectra of $MgFe_2O_4/CuO/TiO_2$ nanocomposite (Fig. 2) showed an absorption peak at 442 nm. The optical characteristics of nanocomposite were determined by studying the absorption spectra.

$$\text{Energy band gap} = E_g = h\nu = \frac{hc}{\lambda}$$

The optical band gap for TiO_2 nanoparticles was calculated using the following equation:

$$(\alpha h\nu)^n = A\,(h\nu - E_g)$$

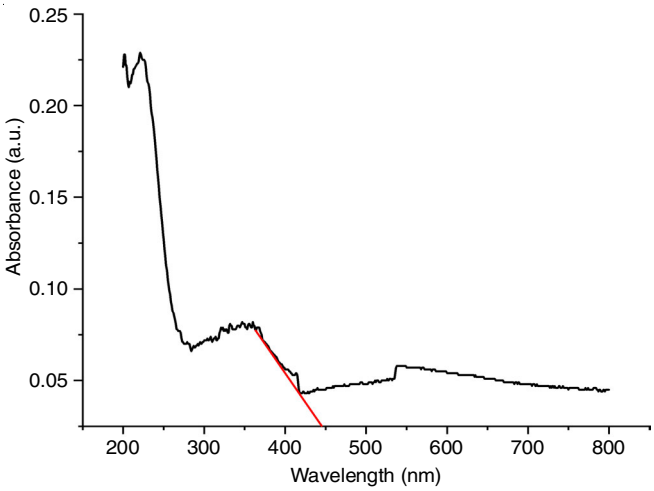

Fig. 2. UV-visible absorption spectrum of $MgFe_2O_4/CuO/TiO_2$ nanocomposite

where α is the absorption coefficient; hν is the photon energy; A is a constant relative to material and n is either 2 for a direct band gap material or ½ for an indirect band gap material. Using the equation, the optical band gap for the absorption peak may be calculated by projecting the linear section of the $(\alpha h\nu)^n$ *vs.* hν curve to zero. The energy band gap of absorption spectra of $MgFe_2O_4/CuO/TiO_2$ nanocomposite in UV was found to be 2.3002 eV (Fig. 3).

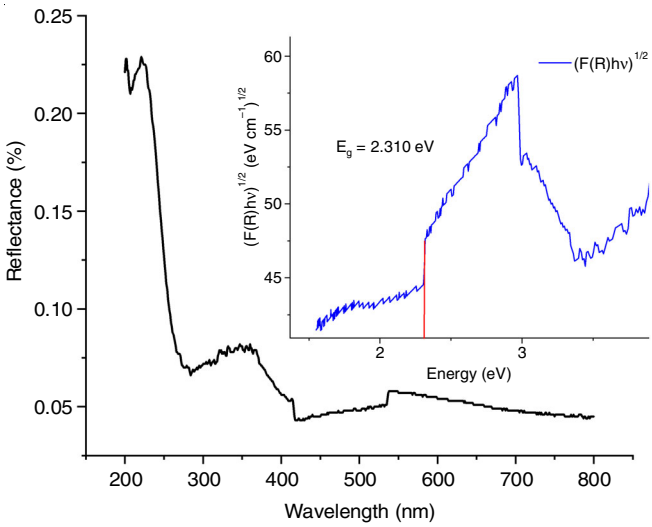

Fig. 3. Band gap of $MgFe_2O_4/CuO/TiO_2$ nanocomposite

Morphological studies

SEM and EDAX: The catalytic activity of the material depends upon their size and surface morphology. As shown in SEM images (Fig. 4a-c), the ternary $MgFe_2O_4/CuO/TiO_2$ nanocomposite was substantially distributed and all the particles were thoroughly mixed in the ternary nanocomposite. The

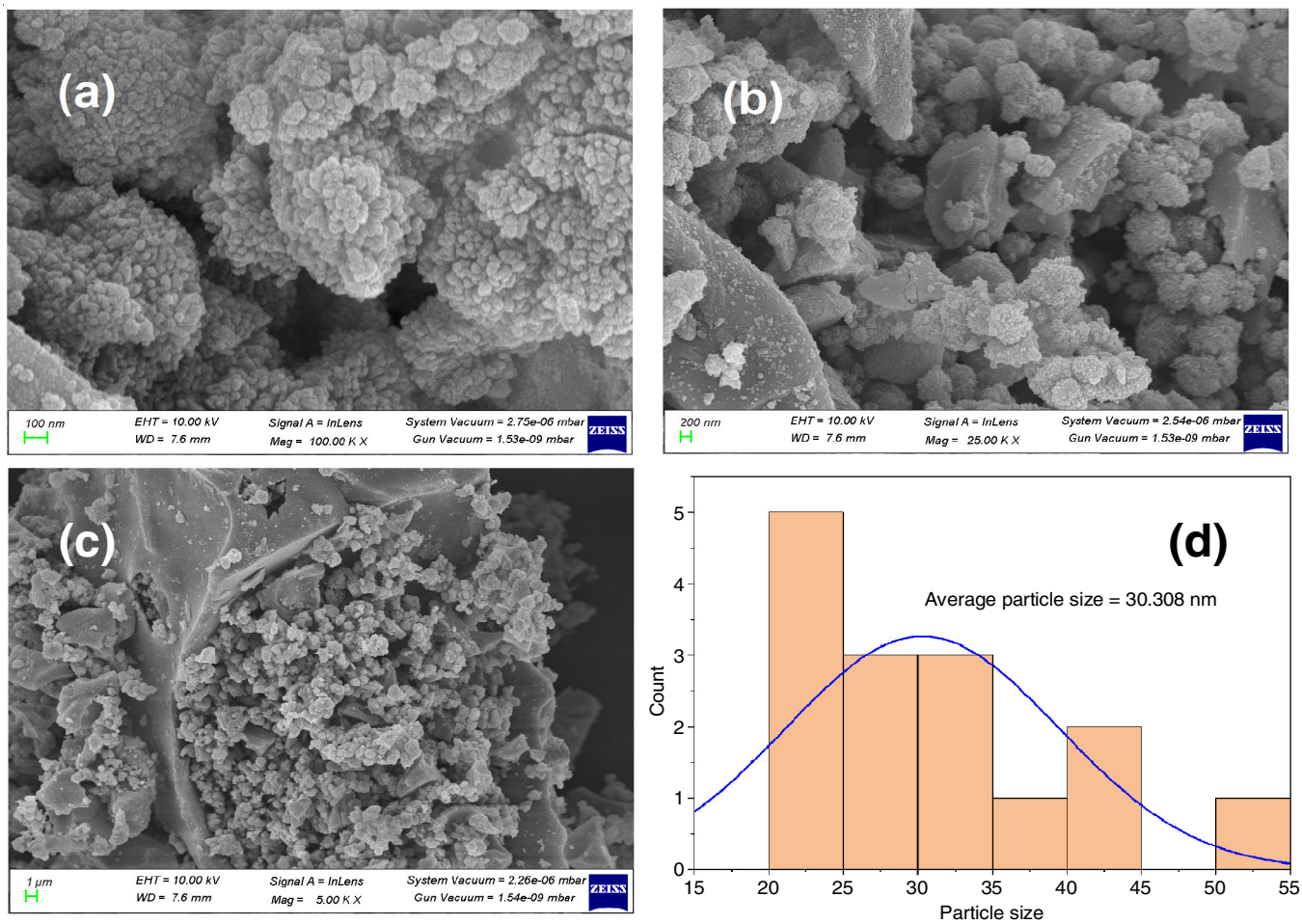

Fig. 4. SEM images of $MgFe_2O_4/CuO/TiO_2$ (a) 100 nm (b) 200 nm (c) 1 µm (d) particle size distribution of $MgFe_2O_4/CuO/TiO_2$

particles are primarily spherical and the ferrite and CuO NPs were evenly distributed across the TiO_2. The average particle size is around 30.308 nm (Fig. 4d). The presence of Mg, Fe, Ti, Cu and O elements is confirmed by an energy-dispersive X-ray spectroscopy (EDX) spectrum (Fig. 5). These results imply that the samples were adequately processed and hence indirectly confirm the formation of nanocomposite.

TEM studies: The structure of the ternary $MgFe_2O_4/CuO/TiO_2$ nanocomposite was further investigated by HR-TEM images. Fig. 6 shows that the particles of the ternary composite are found to be spherical. A lattice fringe with inter-planar distances of 0.24 nm is found in high-resolution TEM images. Fig. 6a shows that all the particles are less than 20 nm. The

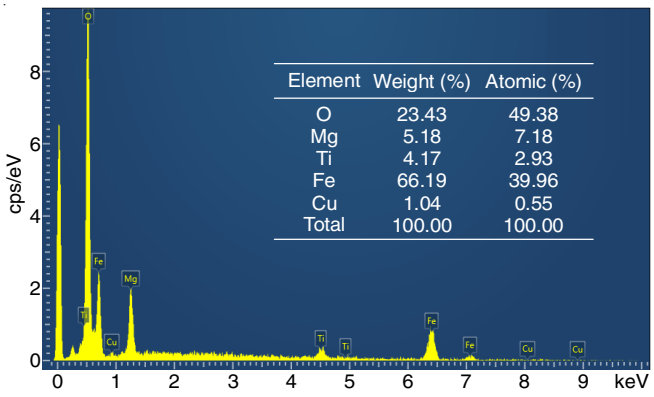

Fig. 5. EDX spectrum of $MgFe_2O_4/CuO/TiO_2$

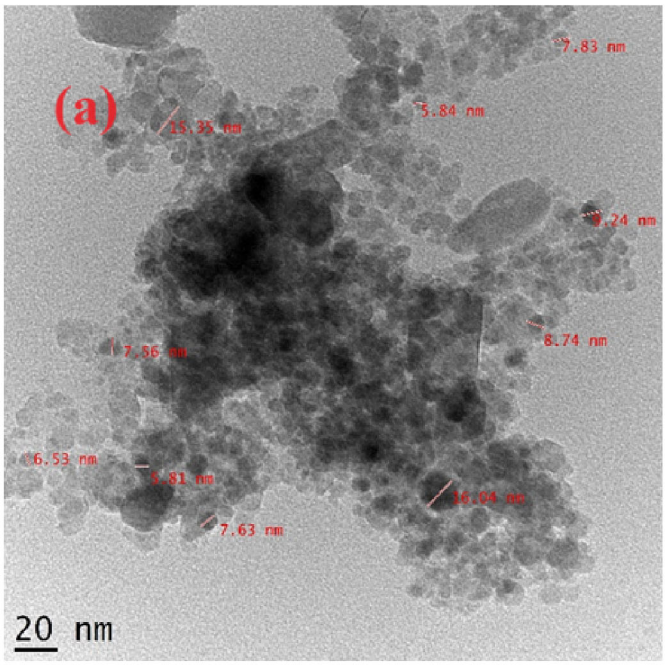

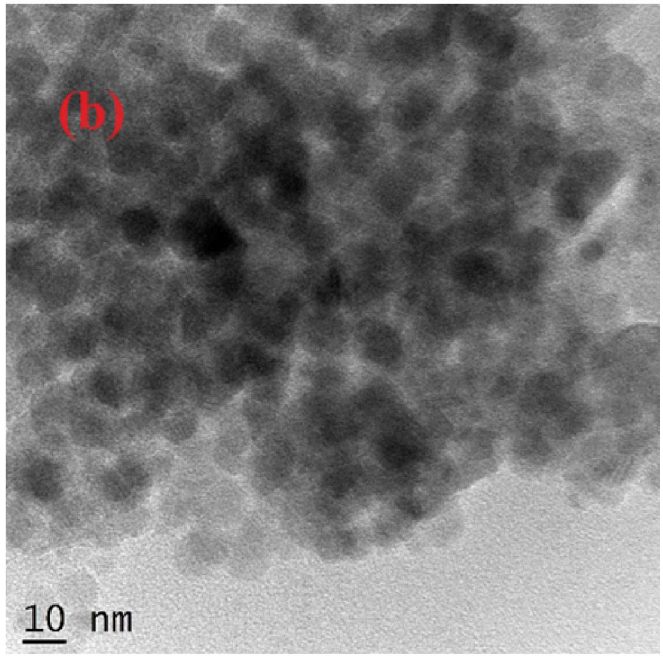

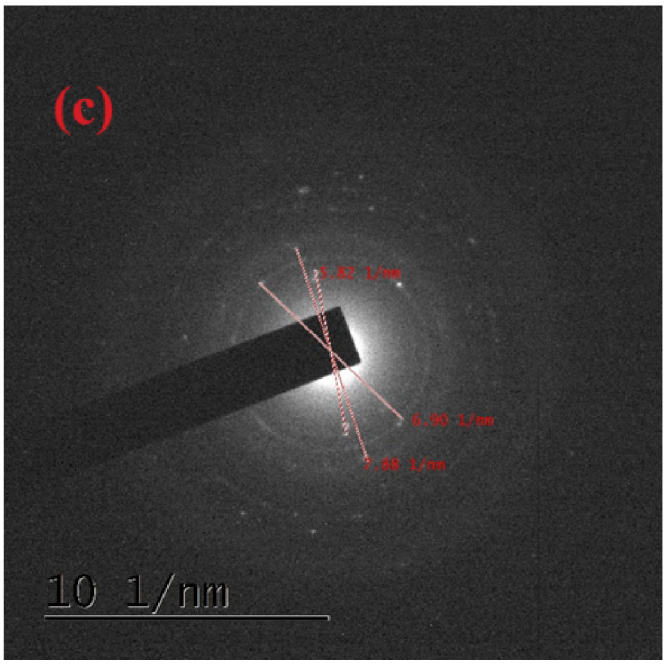

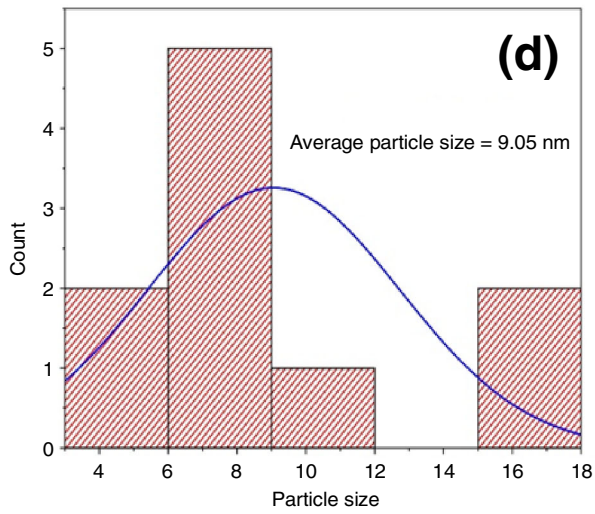

Fig. 6. TEM images of $MgFe_2O_4/CuO/TiO_2$ (a) 20 nm (b) 10 nm (c) SAED pattern (d) particle size distribution of $MgFe_2O_4/CuO/TiO_2$

particle size distribution histogram derived by the Gaussian fitting method (Fig. 6d) verified that the average particle size of $MgFe_2O_4/CuO/TiO_2$ nanocomposite is 9.05 nm.

FT-IR spectral studies: Fig. 7 depicts the FTIR spectrum of synthesized $MgFe_2O_4/CuO/TiO_2$ nanostructures. The bands at 2879 cm^{-1} and 3730 cm^{-1} are the symmetric and asymmetric stretching vibrations of the O-H bond, respectively. The existence of bands at 512 cm^{-1} implies the bending vibration of the Cu-O bond. The appearance of the peak at 1681 cm^{-1} suggests stretching vibration of the Cu-O bond of copper(II) oxide. The 603.01 cm^{-1} frequency range relates to the intrinsic stretching vibrations of metal-oxygen (Fe-O) at tetrahedral sites, whereas the 418.65 cm^{-1} frequency band is connected to metal-oxygen (Ti-O-Ti) stretching vibrations at octahedral sites.

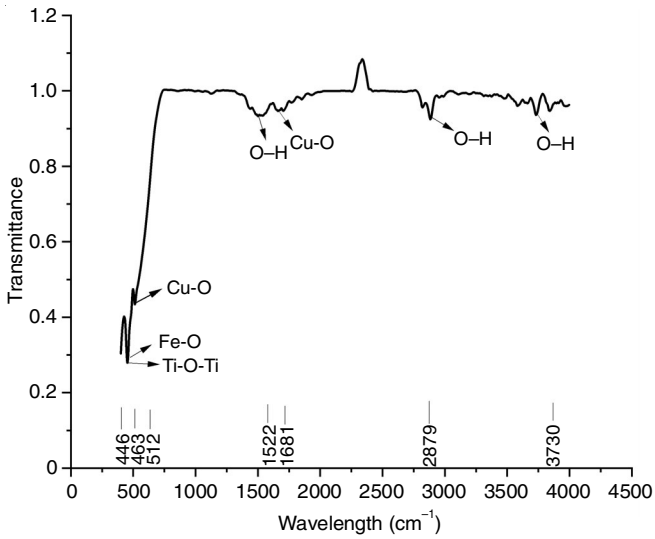

Fig. 7. FTIR spectrum of $MgFe_2O_4/CuO/TiO_2$ nanocomposite

Magnetic properties: Fig. 8 depicts room-temperature magnetization curves of as-synthesized $MgFe_2O_4/CuO/TiO_2$ nanostructures. The saturation magnetization of $MgFe_2O_4/CuO/TiO_2$ nanostructure is 33 emu/g, making them appropriate for the magnetic separation of photocatalytic particles. As a result, these materials have the potential to be used in water treatment operations with little secondary pollution.

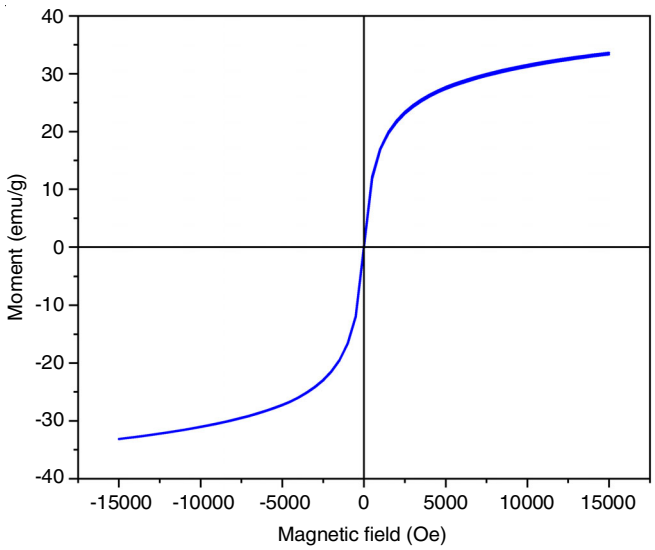

Fig. 8. Magnetization loop for $MgFe_2O_4/CuO/TiO_2$ composite at room temperature

Optimization of photocatalyst activity: The ternay $MgFe_2O_4/CuO/TiO_2$ nanocomposite was investigated for the photocatalytic degradation of malachite green (MG) dye in an aqueous solution under visible light, optimized parameters for the degradation.

Effect of initial dye concentration: The initial concentration of dye was ranged from 5 to 100 ppm, while the catalyst dose remained constant at 500 mg, aiming to determine the optimal dye concentration. The degradation efficiency improved as the dye solution concentration rose from 5 to 100 ppm. However, the degradation tendency is reduced as the dye concentration reaches a certain level. Increased dye molecules may produce fewer active spots on the composite material's surface for a given weight. The results (Fig. 9) show that the optimal starting concentration of MG dye was 10 ppm, at which time the photocatalytic activity reached 100% after 120 min.

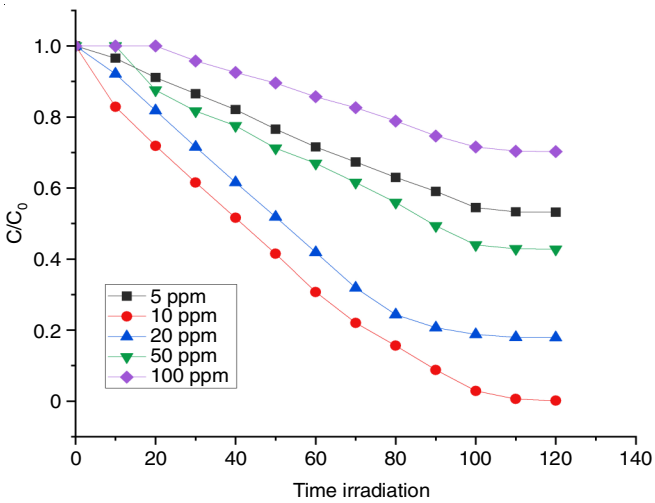

Fig. 9. Effect of initial dye concentration on the photocatalytic degradation of Malachite green dye, catalyst load = 500 mg

Effect of pH of initial dye solution: The impact of pH on the photocatalytic degradation of MG dye using ternary $MgFe_2O_4/CuO/TiO_2$ nanocomposite as photocatalyst at the pH levels ranging from 2 to 10. Fig. 10 illustrates that the photocatalytic degradation rates were maximum at pH 6 and pH 8. In acidic solutions (pH < 6), the dye's photodegradation is slowed by high proton concentrations, leading to reduced degradation efficiency. The optimal pH range of 6-8 resulted in the 100% degradation efficiency after 80 min.

Effect of temperature: The degradation of malachite green dye was observed at four different temperatures (25 ºC, 35 ºC, 45 ºC and 55 ºC) while other parameters remained constant. Increasing the reaction temperature improved the photodegradation efficiency of MG dye on the photocatalyst. Fig. 11 shows that the deterioration efficiency is 100% for all temperatures (25 ºC, 35 ºC, 45 ºC and 55 ºC) but across various periods. The results demonstrate that the MG dye's optimum temperature was 35 ºC, at which point the photocatalytic activity reached 100% after 50 min.

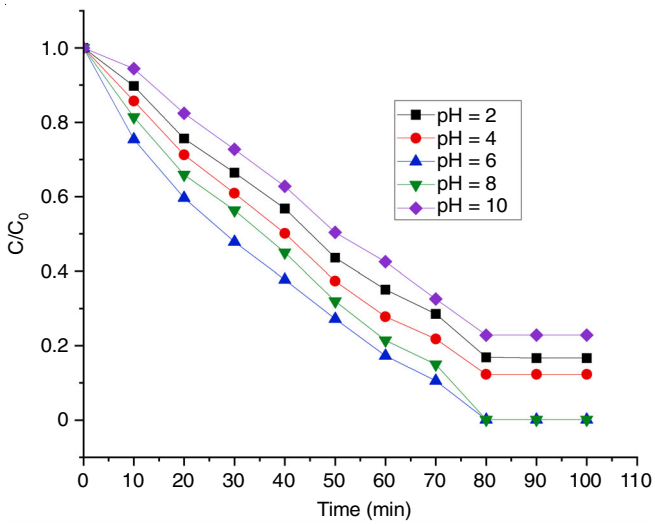

Fig. 10. Effect of pH on initial dye solution; catalyst load = 500 mg, [Dye] =10 ppm (fixed)

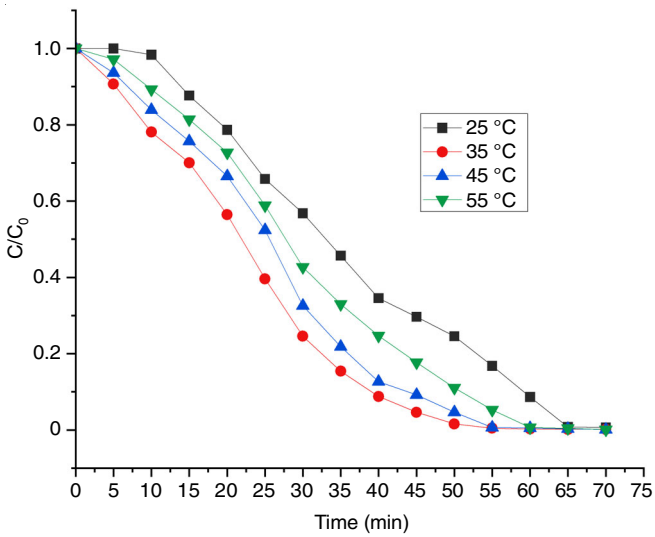

Fig. 11. Effect of temperature on visible light-induced photocatalytic degradation of malachite green; catalyst load = 500 mg, [Dye] = 10 ppm (fixed), pH = 7 (fixed)

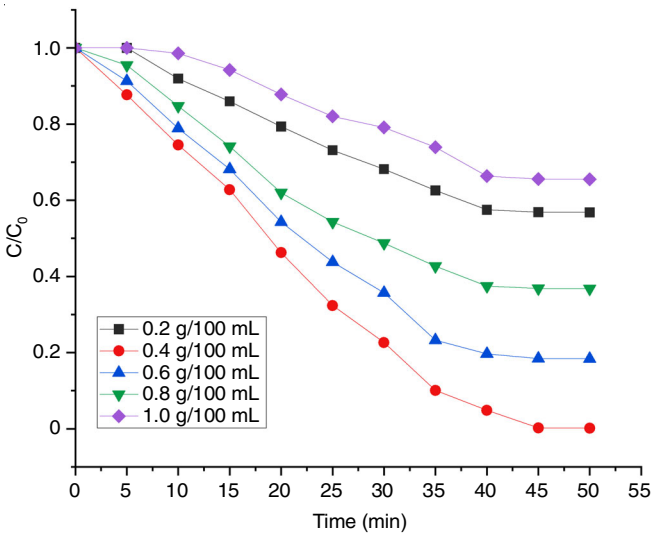

Fig. 12. Effect of catalyst loading on the degradation efficiency of malachite green under visible light irradiation, catalyst load = 500 mg, [Dye] = 10 ppm (fixed), pH = 7 (fixed), temperature = 35 ºC (fixed)

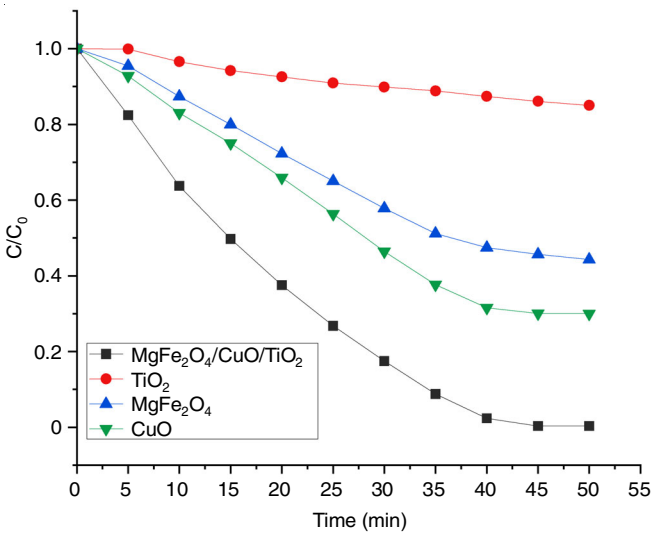

Fig. 13. Plots of C/C_0 of Malachite green for CuO, TiO_2, $MgFe_2O_4$ and $MgFe_2O_4$-CuO-TiO_2 photocatalysts

Effect of catalyst loading: The effect of photocatalyst load on photocatalytic degradation of malachite green dye is investigated using $MgFe_2O_4$/CuO/TiO_2 nanocomposite. The dosage ranged from 200 to 1000 mg/100 mL of dye solution and all observations were conducted at room temperature. From Fig. 12, it was observed that after 45 min, the degradation efficiency was 100% for 400 mg of catalyst.

Effect of irradiation time: Another factor influencing photocatalytic performance for MG dye removal by TiO_2, CuO, $MgFe_2O_4$ and $MgFe_2O_4$-CuO-TiO_2 nanocatalysts is irradiation time. The experiment is conducted at pH 7, with irradiation periods ranging from 0 to 55 min, while all other parameters remain constant. Fig. 13 shows the results of degradation efficiency (C/C_0) *vs*. irradiation time. The degradation efficiency of the synthesized ternary photocatalyst for MG dye increased with an irradiation duration of up to 45 min and then stayed constant. The optimal irradiation period for all samples was 45 min, resulting in dye removal efficiency of 14.9%, 55.6%, 69.9% and 99.6% for TiO_2, CuO, $MgFe_2O_4$ and $MgFe_2O_4$-CuO-TiO_2 catalysts, respectively.

Reusability of catalyst: The reusability of the ternary photocatalyst ($MgFe_2O_4$/CuO/TiO_2 nanocomposite) is also investigated under the optimal circumstances. Following the reaction, the catalyst was collected and cleaned with distilled water and ethyl alcohol. The produced sample's reusability is examined by recycling the composite three times using MG concentration profiles. The dye MG removal efficiency is 83% in the first run, 75% in the second run and 64% in the third run, as seen in Fig. 14. Despite the slight fall in degradation efficiency, the stability of the reused $MgFe_2O_4$/CuO/TiO_2 photo catalysts following MG dye degradation remains considerable.

Antibacterial activity: The disk diffusion method was employed to examine the antibacterial properties of the ternary nanocomposite. It can be observed that the nanocomposite has shown good antibacterial activity against all the selected

TABLE-1
ANTIBACTERIAL ACTIVITY OF THE CATALYSTS

Compounds	Zones of inhibition (diameter in mm), 0.125 µg/mL			
	Gram-positive		Gram-negative	
	Staphylococcus aurues	*Bacillus subtilis*	*Klebsiella pneumoniae*	*Escherichia coli*
$MgFe_2O_4/CuO/TiO_2$	20	24	32	29
Ampicillin	28	36	35	37

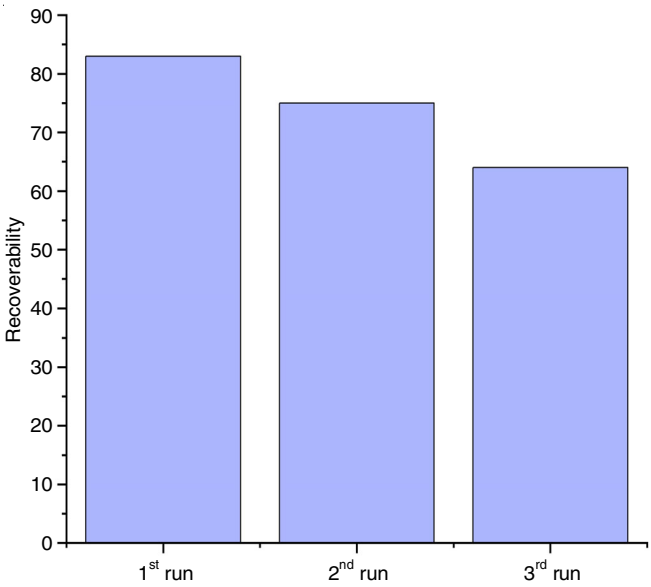

Fig. 14. Reusable capacity of $MgFe_2O_4/CuO/TiO_2$ Nanocomposite of Malachite green

Gram-positive bacteria *S. aureus*, *B. subtilis* and Gram-negative bacteria *E. coli*, *K. pneumonia*. The ternary $MgFe_2O_4/CuO/TiO_2$ nanocomposite has displayed good antibacterial activity, from these studies (Table-1), the most inhibition effect was induced by *S. aureus* which is Gram-positive bacterium.

Conclusion

The ternary nanocomposite comprising $MgFe_2O_4$, CuO and TiO_2 was succesfully prepared using the sol-gel method. The XRD, SEM and UV-visible-DRS analysis demonstrated the formation of crystalline, spherical particles having average crystallite size of 9 nm with a band-gap energy of 2.30 eV. The photocatalytic studies demonstrated that ternary $MgFe_2O_4/CuO/TiO_2$ nanocomposite showed 100% degradation efficiency towards malachite green dye. Under the visible light and UV irradiations, the synthesized $MgFe_2O_4/CuO/TiO_2$ sample with a molar ratio of 0.8:0.1:0.1 demonstrated good catalytic efficiency. An amount of 400 mg of catalyst is for 10 ppm of the dye in 100 mL at 35 ºC at a pH range of 6-8 shown 100 % degradation of malachite green dye. The catalyst could be reused up to three cycles for effective degradation of the dye. The antibacterial activity investigations were done against Gram-positive *Staphylococcus aureus* and *Bacillus subtilis* bacteria and Gram-negative *Escherichia coli*, *Klebsiella pneumonia*, utilizing nanocomposites and the results are comparatively effective with the standard ampicillin antibacterial drug. The novel nanocomposites have shown very efficient photocatalytic activity and better antibacterial activity.

ACKNOWLEDGEMENTS

The authors are thankful to the authorities of Andhra University for the research facilities and Advanced Analytical Laboratory, Andhra University, Visakhapatnam, India for providing the spectral analysis.

CONFLICT OF INTEREST

The authors declare that there is no conflict of interests regarding the publication of this article.

REFERENCES

1. X. Wang, J. Jiang and W. Gao, *Water Sci. Technol.*, **85**, 2076 (2022); https://doi.org/10.2166/wst.2022.088
2. F. Bavarsiha, M. Rajabi and M. Montazeri-Pour, *J. Mater. Sci.: Mater. Electr.*, **29**, 1877 (2018); https://doi.org/10.1007/s10854-017-8098-5
3. C.B. Anucha, I. Altin, E. Bacaksiz and V.N. Stathopoulos, *Chem. Eng. J. Adv.*, **10**, 100262 (2022); https://doi.org/10.1016/j.ceja.2022.100262
4. Y. Ma, M. Ni and S. Li, *Nanomaterials*, **8**, 428 (2018); https://doi.org/10.3390/nano8060428
5. D. Lu, O.A. Zelekew, A.K. Abay, Q. Huang, X. Chen and Y. Zheng, *RSC Adv.*, **9**, 2018 (2019); https://doi.org/10.1039/C8RA09645G
6. O.A. Zelekew, D.-H. Kuo, J.M. Yassin, K.E. Ahmed and H. Abdullah, *Appl. Surf. Sci.*, **410**, 454 (2019); https://doi.org/10.1016/j.apsusc.2017.03.089
7. M. Daous, V. Iliev and L. Petrov, *J. Mol. Catal. A: Chem.*, **392**, 194 (2014); https://doi.org/10.1016/j.molcata.2014.05.020
8. S. Aroob, S.A.C. Carabineiro, M.B. Taj, I. Bibi, A. Raheel, T. Javed, R. Yahya, W. Alelwani, F. Verpoort, K. Kamwilaisak, S. Al-Farraj and M. Sillanpää, *Catalysts*, **13**, 502 (2023); https://doi.org/10.3390/catal13030502
9. S. Pourmoslemi, N. Bayati and R. Mahjub, *J. Sol-Gel Sci. Technol.*, **104**, 320 (2022); https://doi.org/10.1007/s10971-022-05946-2
10. Z. Cao, J. Zhang, J. Zhou, X. Ruan, D. Chen, J. Liu, Q. Liu and G. Qian, *J. Environ. Manag.*, **193**, 146 (2017); https://doi.org/10.1016/j.jenvman.2016.11.039
11. E. Casbeer, V.K. Sharma and X.-Z. Li, *Sep. Purif. Technol.*, **87**, 1 (2012); https://doi.org/10.1016/j.seppur.2011.11.034
12. L.T.T. Nguyen, L.T.H. Nguyen, N.C. Manh, D.N. Quoc, H.N. Quang, H.T.T. Nguyen, D.C. Nguyen and L.G. Bach, *J. Chem.*, **2019**, 3428681 (2019); https://doi.org/10.1155/2019/3428681
13. M. Shahid, L. Jingling, Z. Ali, I. Shakir, M.F. Warsi, R. Parveen and M. Nadeem, *Mater. Chem. Phys.*, **139**, 567 (2013); https://doi.org/10.1016/j.matchemphys.2013.01.058
14. S. Ryali and P.D. Sanasi, *J. Chinese Chem. Soc.*, **65**, 1423 (2018); https://doi.org/10.1002/jccs.201800154
15. W. Li, R. Liang, A. Hu, Z. Huanga and Y.N. Zhou, *RSC. Adv.*, **4**, 36960 (2014); https://doi.org/10.1039/c4ra04768k
16. H. Siddiqui, M.R. Parra, M.S. Qureshi, M.M. Malik and F.Z. Haque, *J. Mater. Sci.*, **53**, 8828 (2018); https://doi.org/10.1007/s10853-018-2179-6